

## Spectral modeling of wave dissipation on negative current gradients

André J. van der Westhuysen\*

Hydraulic Engineering Unit, Deltares, Rotterdamseweg 185, 2629 HD Delft, The Netherlands

### ARTICLE INFO

#### Article history:

Received 4 November 2011  
Received in revised form 2 May 2012  
Accepted 7 May 2012  
Available online 31 May 2012

#### Keywords:

SWAN  
Waves  
Wave-current interaction  
Dissipation

### ABSTRACT

Hindcast studies for the Dutch Wadden Sea using the spectral wind wave model SWAN have shown the significant influence of currents on wave predictions in the tidal inlets. In a number of cases with strong gradients in opposing, partially blocking current, wave heights are significantly overestimated. Ris and Holthuijsen (1996) propose that such overestimations are due to insufficient steepness dissipation of waves on an opposing current gradient. The present paper presents a new formulation for the enhanced breaking dissipation of waves on negative current gradients (accelerating opposing current; decelerating following current). Nonlinear effects are not included in detail for these partial blocking conditions, but handled parametrically. Unlike the expression by Ris and Holthuijsen (1996), the proposed expression isolates the steepening effect of the current gradient on the waves, so that inherently steep young wind sea is not overly dissipated. This expression contains one additional unknown parameter, which was calibrated using laboratory observations. Validation of this enhanced dissipation term for field cases of the Ameland Zeegat tidal inlet (Dutch Wadden Sea) shows an improvement in the tidal channel for both opposing and following current situations with negative gradients. In particular, the results for the young wind sea on the tidal flats are not significantly affected, as desired, unlike with the expression of Ris and Holthuijsen (1996). However, since the remaining dissipation terms in SWAN have been calibrated without this enhanced dissipation term, the addition of the proposed formulation results in some deterioration of the overall statistics.

© 2012 Elsevier B.V. All rights reserved.

### 1. Introduction

The spectral wind wave model SWAN (Booij et al., 1999) is widely used for the computation of wave fields over shelf seas, complex coastal areas and in shallow lakes. The accurate estimation of the nearshore wave processes in this model is important to various applications in these environments.

The Dutch Wadden Sea (Fig. 1) is an example of a complex coastal system that poses significant challenges to nearshore wave modeling. The region is enclosed by a series of barrier islands and the mainland coasts of the provinces of Friesland and Groningen. Tidal inlets are found between the barrier islands, each featuring an ebb tidal delta, one or more main tidal channels, and a complex system of smaller channels and flats extending into the Wadden Sea interior. Apart from the tidal channels, the Wadden Sea interior is shallow and flat, with tidally-modulated depths normally ranging between 0 m (drying) and 3 m.

The Ameland Zeegat tidal inlet (Fig. 2) is found between the barrier islands of Terschelling (to the west) and Ameland (to the east). A program of wave monitoring has been running in this inlet since 2003 (Zijdeveld and Peters, 2008). Hindcast studies with SWAN based on

this data (Groeneweg et al., 2008; Van Vledder et al., 2008) have shown the significant influence of currents on the prediction of wave fields in this tidal inlet. In a number of cases where strong current gradients are found, typically for strong, partially blocking opposing current, wave heights are significantly overestimated. This affects the reliability with which these predictions can be applied in the assessment of safety against flooding, or other geophysical applications in such regions. This issue is addressed in the present study.

The influence of currents on wave fields are typically divided into effects on the wave kinematics and dynamics (Jonsson, 1990). The influence of currents on wave kinematics include effects on the wave phase velocity and the wave number and wavelength. For example, waves traveling over a horizontally sheared current field experience current-induced refraction (e.g. Holthuijsen and Tolman, 1991). The effect of currents on the wave dynamics is described by the action balance equation, given by (1) below. Waves propagating into an opposing current gradient with increasing strength (a negative current gradient) will experience an increase in wave height, which, together with a reduction in wave length, may cause steepness-induced breaking. Conversely, an accelerating following current (positive gradient) results in a reduction in wave height. Note in this regard that a following current that decelerates also constitutes a negative gradient. When a wave field meets an opposing current with a velocity that approaches the wave group velocity, waves are blocked. Here the ray theory embodied in (1) predicts an infinite wave amplitude (singularity), and hence nonlinear effects need to be taken into account

\* UCAR Visiting Scientist at NOAA/NWS/NCEP, 5200 Auth Road, Camp Springs, MD 20746, USA. Tel.: +1 301 673 8000x7041; fax: +1 301 763 8545.

E-mail address: [Andre.VanderWesthuysen@noaa.gov](mailto:Andre.VanderWesthuysen@noaa.gov).

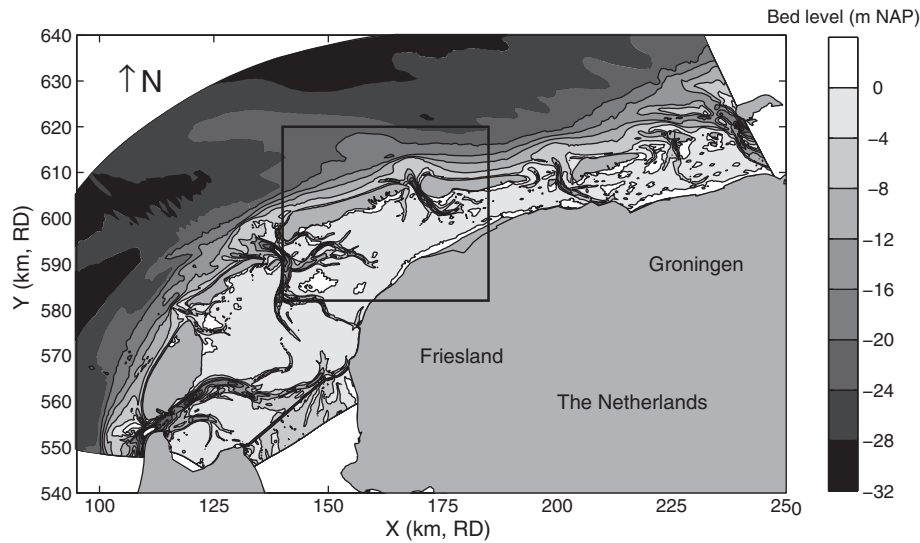


**Fig. 1.** Bathymetry of the Dutch Wadden Sea in the north of the Netherlands, with depths in m below NAP (Dutch leveling datum). Rectangle indicates the location of the Amelander Zeegat region (detail in Fig. 2). Projection in Dutch RD system.

(e.g. Whitham, 1974). These so-called near field conditions will not be considered here.

When currents interact with waves that are actively forced by wind, additional effects are found (Haus, 2007). Wind moving over a wave field in ambient opposing current will have a higher speed relative to the waves (a lower effective wave age) than without it, and a lower relative speed in the case of following current, even if the current field is spatially uniform. The result is a respective increase and decrease in the growth rate of the waves. In addition, Haus (2007) shows that wind-driven waves that experience current refraction over a horizontally sheared current can experience a reduction in their growth rate due to a shifting of the (wave-induced) wind stress direction away from the mean wind direction.

In terms of the far field wave-current interaction (away from the blocking point) these kinematic, dynamic and wind growth-related

effects of currents on waves are, in principle, included in the linear kinematic and dynamical equations of SWAN. Booij et al. (1999) present a validation of current-induced shoaling and refraction using analytical expressions. The exception is the dissipative process that accompanies steepening waves in negative current gradients. Ris and Holthuijsen (1996), hereafter RH96, show that SWAN, using the whitecapping expression of Komen et al. (1984), underestimates wave dissipation in such situations, leading to a strong overestimation in the significant wave height. Models for enhanced wave dissipation on opposing current in the far field have been proposed by RH96, Chawla and Kirby (1998, 2002) and Suastika (2004). These authors all assume a bore-based breaker model (either Battjes and Janssen (1978) or Thornton and Guza (1983)) to be appropriate for modeling the dissipation, using the mean wave steepness as governing parameter. However, Chawla and Kirby (1998)

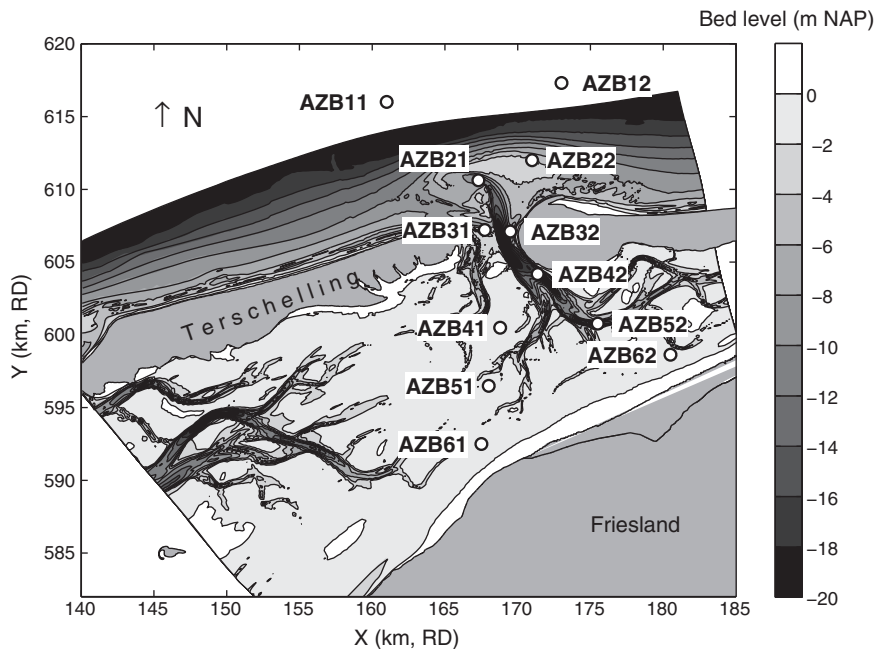


**Fig. 2.** Bathymetry of the Amelander Zeegat region in the Dutch Wadden Sea, including the location of the wave buoys (circles). Depth contours in m below NAP and projection in Dutch RD system.

note, from experimental observation, that current-induced breaking is very different from depth-induced breaking—the breaking is weak and unsaturated, as opposed to the saturated breakers observed in depth-induced breaking. As a practical problem, Ris (1997) reports that the model of RH96 fails under wind wave growth situations, since young wind waves, being inherently steep, are too strongly dissipated. This approach is therefore unsuitable for field situations that feature a combination of wind growth and current interaction, such as in the Dutch Wadden Sea. Hence an alternative approach for the dissipation modeling is required.

The present study aims to develop a formulation for the enhanced dissipation of waves on negative current gradients (both opposing and following currents) in the far field (non-blocking conditions) that can be applied within the context of a spectral model such as SWAN with linear kinematic equations. This expression is to be suitable for both mature waves and young wind sea. The formulation is calibrated and its performance assessed for a range of idealized and field situations.

The present study investigates the application of a saturation-based expression for the far field steepness dissipation of waves on negative current gradients. A number of saturation-based expressions have been proposed in the literature, including Phillips (1985), Alves and Banner (2003), Babanin et al. (2010) and Ardhuin et al. (2010). In the present study, the expression of Alves and Banner (2003), as adapted by Van der Westhuysen (2007), is applied. It will be shown that the proposed calibration settings for this expression, obtained for wind wave growth conditions, yield too little dissipation on opposing current with a negative gradient (as was found for the Komen et al. (1984) expression by RH96 and Chawla and Kirby (2002)). It is, however, conversely not desirable to recalibrate the whitecapping expression to levels sufficient for current-induced steepening at the expense of underprediction for wind wave growth. Hence, a new scaling is proposed that yields enhanced dissipation proportional to the degree of steepening of the wave field due to the negative current gradient. The latter is estimated from the propagation velocity in frequency space  $c_\sigma$ , normalized with the local radian frequency.

In order to investigate the different models for enhanced current-induced dissipation, a data set of 31 cases was assembled. These cases include the flume experiments of Lai et al. (1989), Suastika (2004) and field cases in the Amelander Zeegat during various storms. The data from the two flume experiments are used to calibrate the proposed formulation. The calibrated expression is subsequently validated for deep water, fetch-limited wave growth conditions in the absence of current (showing no influence, as expected), and using field observations in the Amelander Zeegat during three W and NW storms. Since in the Wadden Sea the time scales of energy propagation through the domain are typically shorter than those of the changes in forcing conditions, stationary conditions typically exist here, and will be modeled accordingly.

This paper is structured as follows: Section 2 presents the methodology followed in this study, including a description of the proposed enhanced dissipation expression. Section 3 presents the calibration of this expression, followed by a validation in Section 4. Section 5 closes the paper with conclusions. Appendix A presents a discussion on the model derivation given in Section 2.

## 2. Method

This section presents the methodology of this study. This includes a description of the additions to the action balance equation in SWAN (Section 2.1), the formulations for enhanced current-induced dissipation investigated (Section 2.2), the model settings applied (Section 2.3), the selection of calibration and validation cases (Section 2.4) and the statistical measures used to assess the model performance (Section 2.5).

### 2.1. Additions to the action balance equation

The spectral wind wave model SWAN computes the evolution of wave action density  $N (= E/\sigma$ , where  $E$  is the variance density and  $\sigma$  the relative radian frequency) using the action balance equation:

$$\frac{\partial N}{\partial t} + \nabla_{x,y} \cdot \left[ \left( \vec{c}_g + \vec{U} \right) N \right] + \frac{\partial}{\partial \sigma} (c_\sigma N) + \frac{\partial}{\partial \theta} (c_\theta N) = \frac{S_{\text{tot}}}{\sigma} \quad (1)$$

with the wave kinematics given by the linear expressions (e.g. Mei, 1983):

$$\frac{d \vec{x}}{dt} = \left( \vec{c}_g + \vec{U} \right) = \frac{1}{2} \left[ 1 + \frac{2kd}{\sinh 2kd} \right] \frac{\sigma \vec{k}}{k^2} + \vec{U}, \quad (2)$$

$$\frac{d\sigma}{dt} = c_\sigma = \frac{\partial \sigma}{\partial d} \left[ \frac{\partial d}{\partial t} + \vec{U} \cdot \nabla d \right] - c_g \vec{k} \cdot \frac{\partial \vec{U}}{\partial s}, \quad (3)$$

and

$$\frac{d\theta}{dt} = c_\theta = -\frac{1}{k} \left[ \frac{\partial \sigma}{\partial d} \frac{\partial d}{\partial m} + \vec{k} \cdot \frac{\partial \vec{U}}{\partial m} \right], \quad (4)$$

and the right-hand side given by:

$$S_{\text{tot}} = S_{\text{in}} + S_{\text{wc}} + S_{\text{nl4}} + S_{\text{bot}} + S_{\text{brk}} + S_{\text{nl3}} + \left( S_{\text{wc,cur}} + S_{\text{bot,perf}} \right) \quad (5)$$

The terms on the left-hand side of Eq. (1) represent, respectively, the change of wave action in time, the propagation of wave action in geographical space (with  $\vec{c}_g$  the intrinsic group velocity vector and  $\vec{U}$  the ambient current), the shifting of the relative radian frequency  $\sigma$  due to variations in mean current and depth (with the propagation velocity  $c_\sigma$ ) and depth- and current-induced refraction (with propagation velocity  $c_\theta$  in directional space  $\theta$ ). In Eqs. (2)–(4),  $s$  is the spatial coordinate in the propagation direction  $\theta$ ,  $m$  is a spatial coordinate perpendicular to  $s$ ,  $k$  is the wavenumber vector and  $d$  is the depth. In the present study, we shall only consider stationary simulations, so that  $\partial N/\partial t = 0$  in Eq. (1). The right-hand side of Eq. (1) represents processes that generate, dissipate or redistribute wave energy, given by Eq. (5). In deep water, three source terms are dominant: the transfer of energy from the wind to the waves,  $S_{\text{in}}$ ; the dissipation of wave energy due to whitecapping,  $S_{\text{wc}}$ ; and the nonlinear transfer of wave energy due to quadruplet (four-wave) interaction,  $S_{\text{nl4}}$ . In shallow water, dissipation due to bottom friction,  $S_{\text{bot}}$ , depth-induced breaking,  $S_{\text{brk}}$ , and nonlinear triad (three-wave) interaction,  $S_{\text{nl3}}$ , are additionally accounted for.

In the present study, two additional source terms are included in Eq. (5). These are terms for the enhanced breaking dissipation of waves on a current  $S_{\text{wc,cur}}$ , the subject of this study, and a special dissipation term  $S_{\text{bot,perf}}$  required for the evaluation of the Suastika (2004) laboratory data set (see Section 2.4.2 below).

### 2.2. Models for enhanced breaking dissipation on negative current gradients

Below, various formulations for steepness breaking (whitecapping) are presented. First, the saturation-based whitecapping expression proposed by Van der Westhuysen (2007) is presented. Subsequently, two formulations for enhanced breaking dissipation on negative current gradients are described, namely the expression of RH96 and the formulation proposed in the present study.

#### 2.2.1. Saturation-based whitecapping

Van der Westhuysen (2007) proposes an adapted version of the saturation-based whitecapping formulation developed by Alves and Banner (2003). This expression is combined with the wind input

formulation proposed by Yan (1987). The whitecapping expression of Van der Westhuysen (2007) is composed of two parts, namely a contribution to the dissipation by wave breaking, and a weaker non-breaking contribution:

$$S_{wc,SB}(\sigma, \theta) = f_{br}(\sigma)S_{dis,break} + [1 - f_{br}(\sigma)]S_{dis,non-break}, \quad (6)$$

where the breaking part is based on the saturation-based expression of Alves and Banner (2003), as modified by Van der Westhuysen et al. (2007):

$$S_{dis,break} = -C'_{ds} \left[ \frac{B(k)}{B_r} \right]^{\frac{p}{2}} [\tanh(kd)]^{\frac{2-p}{4}} g^{\frac{1}{2}} k^{\frac{1}{2}} E(\sigma, \theta), \quad (7)$$

and the non-breaking part is based on the pulse-based expression of Komen et al. (1984), providing low-level background dissipation (e.g. for swell):

$$S_{dis,non-break} = -C_{ds} \left( \frac{k}{\bar{k}} \right)^q \left( \frac{\bar{s}}{\bar{s}_{PM}} \right)^r \bar{\sigma} E(\sigma, \theta). \quad (8)$$

The weighting factor  $f_{br}$  determines the changeover from the dissipation of breaking to non-breaking waves. This weighting is a function of the ratio between the spectral saturation  $B(k)$  and a threshold saturation level  $B_r$ :

$$f_{br}(\sigma) = \frac{1}{2} + \frac{1}{2} \tanh \left\langle 10 \left( \left[ \frac{B(k)}{B_r} \right]^{\frac{1}{2}} - 1 \right) \right\rangle \quad (9)$$

Over the spatial scales considered in the field cases of the present study, only the component Eq. (7) in the expression (6) is relevant. The parameter  $p$  is a function of the inverse wave age  $u_*/c$ , based on scaling arguments involving a spectral balance between the wind input, whitecapping and nonlinear interaction terms (see Van der Westhuysen et al. (2007) for details):

$$p(u_*/c) = 3 + \tanh \left[ 25 \left( \frac{u_*}{c} - 0.1 \right) \right] \quad (10)$$

In Van der Westhuysen (2007) the remaining parameters of Eq. (7) were calibrated to  $C'_{ds} = 5.0 \times 10^{-5}$  and  $B_r = 1.75 \times 10^{-3}$  respectively.

### 2.2.2. Ris and Holthuijsen (1996)

As discussed in Section 1, RH96 show that the default, pulse-based whitecapping expression of Komen et al. (1984) does not provide sufficient wave breaking dissipation in situations of strong negative current gradients, such as found under partial blocking conditions. They demonstrate that the addition of a dissipation term based on the bore-based breaker model of Battjes and Janssen (1978) to Eq. (5) is effective in the modeling of the rapid dissipation occurring near the blocking point. This expression reads:

$$S_{wc,cur}(\sigma, \theta) = -C'_{ds,RH} Q_b \left( \frac{s_{max}}{\bar{s}} \right)^2 \bar{\sigma} \frac{k}{\bar{k}} E(\sigma, \theta), \quad (11)$$

where  $\bar{s} = \bar{k} \sqrt{E_{tot}}$  is the mean wave steepness,  $\bar{\sigma}$  the mean relative radian frequency, given by

$$\bar{\sigma} = E_{tot}^{-1} \int_0^{2\pi} \int_0^{\infty} \sigma E(\sigma, \theta) d\sigma d\theta \quad (12)$$

and  $\bar{k}$  the mean wave number, defined as

$$\bar{k} = \left( E_{tot}^{-1} \int_0^{2\pi} \int_0^{\infty} \frac{1}{\sqrt{k}} E(\sigma, \theta) d\sigma d\theta \right)^{-2}. \quad (13)$$

The proportionality coefficient  $C'_{ds,RH} \equiv \alpha_{BJ} = 1$ . The variable  $Q_b$  is the fraction of breaking waves, determined by

$$\frac{1 - Q_b}{\ln Q_b} = -8 \frac{E_{tot}}{H_m^2} \quad (14)$$

in which a maximum wave height  $H_m$  is defined based on a limiting steepness

$$H_m = \frac{2\pi s_{max}}{k} \quad (15)$$

The limiting steepness  $s_{max}$  is set to 0.14, based on Miche's criterion for the limiting steepness of an individual breaker. We note that Chawla and Kirby (1998) show that when propagating on an opposing current, waves can break at a lower steepness than this. RH96 demonstrate that expression (11) enhances the dissipation for waves exceeding a mean steepness of  $\bar{s} = 0.08$ , as such can occur on strong negative current gradients.

### 2.2.3. Enhanced saturation-based dissipation

Chawla and Kirby (2002) show that, as an alternative to the bore-based expression proposed by RH96, wave dissipation on negative current gradients can be modeled using a conventional whitecapping expression of the form Eq. (8) with an enhanced proportionality coefficient  $C_{ds}$ . A number of studies (e.g. Alves and Banner, 2003; Ardhuin et al., 2010; Van der Westhuysen et al., 2007) have discussed the restrictions of the whitecapping form Eq. (8), in favor of a saturation-based approach. Consequently, the basic form of the saturation-based whitecapping expression (7) is applied here to model the enhanced dissipation due to wave-current interaction, included as  $S_{wc,cur}$  in Eq. (5). We start by assuming that the degree of enhancement of the whitecapping term Eq. (7) should scale with the relative increase in the wave steepness due to the current gradient, over the time scale of that steepening. This can be expressed as  $\frac{ds^*}{dt} / S^*$ , where  $S^*$  is the steepness spectrum given by:

$$S^*(\sigma) = kE(\sigma)^{\frac{1}{2}} \quad (16)$$

For simplicity, deep water conditions are assumed, being applicable to the tidal channels that this model is mainly intended for. The normalized rate of increase in the wave steepness can then be expressed as:

$$\frac{dS^*}{dt} / S^* = \frac{1}{\sigma^2 E^{\frac{1}{2}}} \left[ \sigma^2 \frac{dE^{\frac{1}{2}}}{dt} + E^{\frac{1}{2}} \frac{d\sigma^2}{dt} \right] = \frac{1}{2} \frac{dE}{dt} / E + 2 \frac{d\sigma}{dt} / \sigma \quad (17)$$

Hence, the normalized rate of increase in wave steepness is dependent on both the rate of increase of the energy density  $E$  and the rate of increase of  $\sigma$ , namely the dynamic and kinematic effects of the current respectively.

To isolate the effect of the current gradient, we make the further approximation that the source terms in Eq. (1) are weak relative to the effect of the current gradient over the limited spatial scales that the latter acts. Therefore, over this limited domain, the action flux  $F_{const}$  would be approximately constant along a wave ray:

$$(c_g + U_s)N = (c_g + U_s) \frac{E}{\sigma} = F_{const} \quad (18)$$

where  $U_s$  is the current velocity component in the direction of the wave propagation. Considering the situation away from the blocking point ( $c_g \gg U_s$ ), we have (deep water):

$$E = \frac{2}{g} F_{const} \sigma^2 \quad (19)$$

Substituting Eq. (19) in Eq. (17), the first term on the RHS of Eq. (17) can be related to the rate of change of  $\sigma$ :

$$\frac{dS^*}{dt} / S^* = \frac{1}{2} \left( 2 \frac{d\sigma}{dt} / \sigma \right) + 2 \frac{d\sigma}{dt} / \sigma = 3 \frac{d\sigma}{dt} / \sigma \quad (20)$$

Hence, the normalized rate of increase in steepness due to the current gradient can be related exclusively to  $(d\sigma/dt)/\sigma = c_{\sigma}/\sigma$ , where  $c_{\sigma}$  is given by Eq. (3).

Note that the overall steepening expressed in Eq. (17) is also affected by processes such as wind wave growth that influence  $E$  directly. This implies that if wave steepness itself would be used as a predictor for modeling enhanced current-induced dissipation (as in RH96), it would erroneously include the effect of these additional wave steepening processes as well. In Section 4.1 we will show that this leads to unintended dissipation of young wind fields, for example. In view of this, in the proposed model  $c_{\sigma}/\sigma$  is used to isolate the normalized rate of increase in steepness due to the current alone.

Of the processes contained in Eq. (3), a negative gradient in the current  $\bar{U}$  (last term on RHS) is considered to be the largest contributor to positive values of  $c_{\sigma}$ , and hence an increase in steepness according to Eq. (20), see analysis in Appendix A (Battjes, 2011). Note also from this analysis that such negative gradients can occur under both opposing and following currents. Observations of wave dissipation on negative current gradients in the literature are mostly limited to opposing current cases (e.g. Chawla and Kirby, 2002; Lai et al., 1989; Suastika, 2004). To our knowledge, the flume experiment of Babanin et al. (2011) are the only observations featuring a negative current gradient in following current. Their results indeed show that waves steepen on a decelerating following current, which can lead to breaking dissipation.

Based on the above, we scale the whitecapping expression (7) with  $c_{\sigma}/\sigma$  to obtain enhanced dissipation for negative gradients in both opposing and following currents. Dimensional analysis then yields:

$$S_{wc,cur}(\sigma, \theta) = -C_{ds}^* \max \left[ \frac{c_{\sigma}(\sigma, \theta)}{\sigma}, 0 \right] \left[ \frac{B(k)}{B_r} \right]^{\frac{p}{2}} E(\sigma, \theta). \quad (21)$$

As above, deep water conditions are assumed, so that the shallow water scaling factor  $[\tanh(kd)]^{\frac{2-p}{2}}$  in Eq. (7) is dropped. This term is only relevant under conditions where dissipation is due to wind sea growth. The dissipation modeled with Eq. (21) is determined by the spectral saturation level  $B(k)$  as a ratio of the threshold level  $B_r$  as in Eq. (7), but is enhanced by the factor  $c_{\sigma}/\sigma$ . The enhanced dissipation is not required in situations of positive current gradients, where the elongating waves do not experience increased breaking. This is achieved with the maximum function, so that only frequency upshifts are taken into account. In the absence of direct observations, the parameterizations of  $B_r$  and  $p$  are taken similar to those of Eq. (7). Hence, Eq. (21) contains one additional calibration parameter relative to Eq. (7), namely the proportionality coefficient  $C_{ds}^*$ . The calibration of this parameter is considered in Section 3.

### 2.3. Model settings

The computations presented here were performed using the SWAN model version 40.72ABC, in stationary third-generation mode. For the deep water physics, the combination of wind input  $S_{in}$  and saturation-based whitecapping  $S_{wc}$  of Van der Westhuysen (2007), presented in Section 2.2.1, was applied. Quadruplet nonlinear interaction  $S_{n14}$  was modeled using the Discrete Interaction Approximation (DIA) of Hasselmann et al. (1985). The shallow water source terms include triad nonlinear interaction  $S_{n13}$  according to Eldeberky (1996) and bottom friction according to Hasselmann et al. (1973), both with their default settings in SWAN. For depth-induced breaking

$S_{brk}$ , the biphasic breaker model of Van der Westhuysen (2010) was applied, with the extension proposed by Van der Westhuysen (2009). In the Amelander Zeegat field cases, wave diffraction, which may redistribute the energy of waves steepened by the current geographically, is taken into account with the phase-decoupled diffraction expression of Holthuijsen et al. (2003). Hereafter, these settings will be referred to as the default model. Two further variants are studied, featuring the additional expressions for enhanced current-induced dissipation of RH96 given by (11) and the proposed expression (21). The convergence criteria applied are the so-called curvature-based criteria proposed by Zijlema and Van der Westhuysen (2005).

### 2.4. Data sets

In order to calibrate and assess the performance of the proposed expression for wave dissipation on opposing current, a data set of partially blocking laboratory flume cases (calibration) and field cases (validation) have been assembled. These are presented below.

#### 2.4.1. Lai et al. (1989) flume experiment

Lai et al. (1989) investigated the transformation of the wave spectrum on a strong negative current gradient in a flume of 8 m length and 0.75 m depth. An opposing current flow was induced along the flume, which was contracted by the presence of a shoal, resulting in an increase in the current velocity from  $U = -0.13$  to  $-0.22$  m/s. Random, long-crested waves were mechanically generated at the downstream end of the flume. In the case considered here, the incident wave field had a significant wave height of  $H_{m0} = 0.019$  m and a mean period of  $T_{m01} = 0.5$  s. This represents a partial blocking situation with  $U/c_{g, peak} = 0.52$ , which resulted in a strong reduction in the observed significant wave height over the shoal, in combination with an increase in the absolute mean wave period  $T_{m01}$ .

#### 2.4.2. Suastika (2004) flume experiment

Suastika et al. (2000) and Suastika (2004) studied partial and full wave blocking using a 35 m long flume, with a 12 m measurement section at its center. Three of these cases are considered here, all involving partial blocking with  $U/c_{g, peak} = 0.47$  to best represent the conditions in the Dutch Wadden Sea (Table 1). Random waves (JONSWAP spectrum) were mechanically generated at the one end of the flume, while a water head difference induced an opposing current flow along the flume. At the measurement section, the flow was contracted by a false wall and perforated bottom to create a sump for suction pumps. Here water was gradually withdrawn through the bottom of the flume, creating an opposing current that reduced approximately linearly to zero in the up-wave direction (negative gradient). However, the presence of this perforated false bottom had the disadvantage of introducing an additional source of dissipation, that must be added to Eq. (5). The dissipation due to the interaction between the waves and the false bottom is given by:

$$S_{bot,perf}(\sigma, \theta) = -2\mu_b c_g E(\sigma, \theta) \quad (22)$$

where  $\mu_b$  is a coefficient that is dependent on the wave height and period, which was empirically estimated by Suastika (2004). This source

**Table 1**  
Selected cases from the laboratory flume experiment of Suastika (2004).

Case	$Q$ ( $m^3/s$ )	$H_{m0}$ (m)	$T_p$ (s)
1100suast003	0.078	0.2	1.1
1100suast002	0.078	0.5	1.1
1100suast004	0.078	0.8	1.1

of dissipation, which is significant, is accounted for in the simulations for this experiment, but is irrelevant for general application.

#### 2.4.3. Amelander Zeegat

Conditions in the Dutch Wadden Sea are represented by a collection of 27 stationary cases taken from NW and W storms occurring over the Amelander Zeegat during 2007. The NW storms feature high water levels of up to 2.6 m NAP (Dutch Leveling Datum) combined with wind speeds of up to 18.5 m/s from 320 to 331°N (Table 2). The W storms feature wind speeds of up to 20.3 m/s from 264 to 279°N (Table 3). During the NW events, the wind and offshore waves are directed more or less straight into the tidal channel. Although during W events the wind direction was not parallel to the tidal channel, offshore waves propagate into the tidal inlet by refraction over the ebb tidal delta. During these events, two arrays of wave buoys were placed along transects through the tidal inlet, where strong current gradients are found (Fig. 2). The buoys AZB32, AZB42 and AZB52 in the main channel were well-situated to record conditions of wave-current interaction. Currents were not measured, but computed using the hydrodynamic model Delft3D including tidal, wind and wave forcing, calibrated to water level observations.

#### 2.5. Method of analysis

The predictive ability of the dissipation expressions (11) and (21) was determined on the basis of scatter index and relative bias scores, which were computed for both the significant wave height  $H_{m0}$  and the mean period  $T_{m-1,0}$ . These measures are defined respectively as

$$\text{Rel. bias}_{\Psi} = \frac{\sum_{i=1}^N (\Psi_{\text{SWAN}}^i - \Psi_{\text{obs}}^i)}{\sum_{i=1}^N \Psi_{\text{obs}}^i}, \quad (23)$$

and

$$\text{SI}_{\Psi} = \sqrt{\frac{\frac{1}{N} \sum_{i=1}^N (\Psi_{\text{SWAN}}^i - \Psi_{\text{obs}}^i)^2}{\frac{1}{N} \sum_{i=1}^N \Psi_{\text{obs}}^i}}, \quad (24)$$

where  $\Psi_{\text{obs}}$  is the observed significant wave height  $H_{m0, \text{obs}}$  or mean period  $T_{m-1,0, \text{obs}}$ , and  $\Psi_{\text{SWAN}}$  is the corresponding modeled value  $H_{m0, \text{SWAN}}$  or  $T_{m-1,0, \text{SWAN}}$ , in a sample of size  $N$ . These statistical measures were computed over all cases for a given laboratory or field situation (e.g., Suastika (2004) or Amelander Zeegat). Subsequently, these individual scores were combined with a weighted average (based on the number of cases per situation) to obtain overall scores for, for example, the total validation subset.

**Table 2**

Selected cases for the NW storms recorded during November 2007 in the Amelander Zeegat. Wind speed and direction are spatial averaged observations. Water levels at station AZB11. Current speed and direction are computed values at buoy location AZB42.

Case	Date and time (UTC)	$U_{10}$ (m/s)	$U_{\text{dir}}$ (°N)	WL (m NAP)	$U$ (m/s)	$\theta_c$ (°Cart)
f102am07z016	08/11/2007 18:10	11.8	282	1.3	1.27	322
f102am07z017	09/11/2007 00:10	15.6	323	0.7	0.87	141
f102am07z018	09/11/2007 02:20	15.8	320	0.3	0.75	144
f102am07z019	09/11/2007 04:50	17.3	322	1.5	1.24	322
f102am07z020	09/11/2007 08:10	18.2	325	2.6	0.30	326
f102am07z021	09/11/2007 09:20	18.4	326	2.4	0.69	141
f102am07z022	09/11/2007 11:00	18.5	328	1.7	1.32	138
f102am07z023	09/11/2007 12:30	18.2	331	1.0	1.24	140
f102am07z024	09/11/2007 14:30	18.0	328	0.4	1.28	141
f102am07z025	09/11/2007 17:20	16.8	325	1.0	0.62	312
f102am07z026	09/11/2007 19:10	15.8	331	1.5	0.51	323
f102am07z027	09/11/2007 20:30	15.5	326	1.5	0.22	139

**Table 3**

Selected cases for the W storms recorded during January and March 2007 in the Amelander Zeegat. Wind speed and direction are spatial averaged observations. Water levels at station Nes. Current speed and direction are computed values at buoy location AZB42.

Case	Date and time (UTC)	$U_{10}$ (m/s)	$U_{\text{dir}}$ (°N)	WL (m NAP)	$U$ (m/s)	$\theta_c$ (°Cart)
f102am07z028	11/01/2007 04:00	11.9	237	1.36	1.39	140
f102am07z032	11/01/2007 16:00	14.8	265	1.06	0.58	137
f102am07z033	11/01/2007 16:40	14.8	264	0.95	0.78	140
f102am07z034	11/01/2007 20:40	18.2	268	0.44	0.60	141
f102am07z003	11/01/2007 22:40	18.8	279	1.29	0.44	325
f102am07z006	18/01/2007 17:20	20.3	267	1.43	0.69	326
f102am07z039	18/01/2007 18:00	20.1	268	1.82	0.54	323
f102am07z040	18/01/2007 18:40	19.9	269	2.24	0.29	331
f102am07z042	19/01/2007 07:40	13.1	271	1.45	0.74	323
f102am07z043	19/01/2007 12:00	14.3	272	1.36	1.36	139
f102am07z044	18/03/2007 07:40	14.8	274	1.10	1.03	323
f102am07z045	18/03/2007 09:20	13.8	275	1.76	0.49	324
f102am07z009	18/03/2007 14:40	18.1	266	0.67	1.16	140
f102am07z010	18/03/2007 15:40	17.9	271	0.63	0.83	141
f102am07z011	18/03/2007 17:00	17.1	268	1.17	1.00	324

For the calibration of the dissipation model, a third statistical measure was used, namely a combined error function  $\varepsilon$ . This error function is defined in terms of the scatter indices of  $H_{m0}$  and  $T_{m-1,0}$ , as follows:

$$\varepsilon = \frac{1}{2} (\text{SI}_H + \text{SI}_T) \quad (25)$$

using the definition in (24). As above, this error function was computed over all cases for a given laboratory or field situation. By considering the weighted mean of the error  $\varepsilon$  over a collection of cases, optimal calibration settings were determined for the total calibration subset.

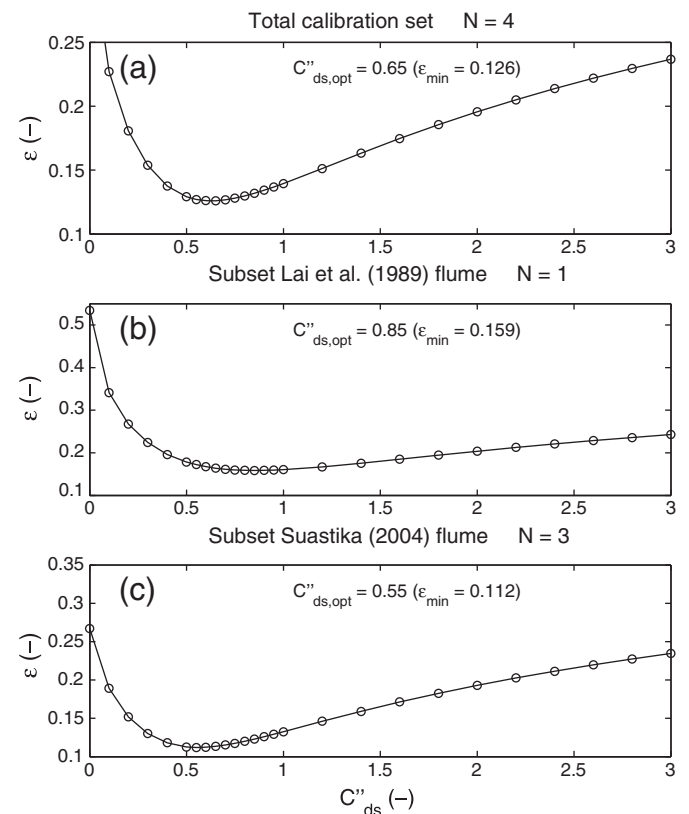


**Fig. 3.** Calibration of (21). Error function  $\varepsilon$  as function of proportionality coefficient  $C''_{ds}$  for various calibration subsets.

### 3. Calibration

The expression for enhanced dissipation Eq. (21) features one calibration parameter, namely the proportionality coefficient  $C_{ds}''$ , the calibration of which is considered in this section. Before this calibration was carried out, the impact of nonlinear effects was estimated using the Stokes third-order dispersion relation of Kirby and Dalrymple (1986). It was confirmed that these are indeed not significant in the partial blocking cases considered here (not shown).

The laboratory flume case of Lai et al. (1989) and the partial blocking cases of Suastika (2004) were used for the calibration of Eq. (21). Fig. 3 presents the calibration of  $C_{ds}''$  by means of the optimization of the error function  $\varepsilon$ , where  $SI_H$  and  $SI_T$  are the scatter indices of  $H_{m0}$  and  $T_{m-1,0}$  respectively. Panels (b) and (c) show that in the individual calibration subsets of Lai et al. (1989) and Suastika (2004) the error  $\varepsilon$  has a local maximum at  $C_{ds}''=0$  and a strong reduction over  $0 < C_{ds}'' < 0.5$ , indicating the importance of including the dissipation term Eq. (21). The calibration result for the total calibration data set (panel (a)) gives an optimal setting of  $C_{ds}''=0.65$ .

Fig. 4 presents the calibration results with  $C_{ds}''=0.65$  along the flume for two representative examples of the laboratory cases, with the results for the RH96 expression included for comparison. The corresponding overall error statistics are given in Table 4. The left-hand panels of Fig. 4 show the calibration results for a partial blocking case of Suastika (2004). Panel (g) shows positive values of the predictor  $c_{\sigma}/\sigma$  along the flume, which corresponds to the negative current gradient (panel (e)) and leads to enhanced dissipation. As a result, a

**Table 4**

Overall statistics of the Suastika (2004) and Lai et al. (1989) calibration cases presented in Fig. 4.  $Rel.bias_H$  and  $Rel.bias_T$  indicate the relative bias in  $H_{m0}$  and  $T_{m01}$ , respectively.  $SI_H$  and  $SI_T$  indicate the corresponding scatter indices.

Case and model variant	$Rel.bias_H$ (-)	$SI_H$ (-)	$Rel.bias_T$ (-)	$SI_T$ (-)
<b>Suastika (2004)</b>				
Default	0.388	0.453	0.009	0.050
RH96	0.223	0.263	0.029	0.055
Proposed model	0.056	0.099	0.057	0.072
<b>Lai et al. (1989)</b>				
Default	0.772	1.029	-0.028	0.040
RH96	0.203	0.320	-0.008	0.025
Proposed model	0.091	0.282	-0.003	0.025

significant improvement in the modeled  $H_{m0}$  is found over that of both the default and RH96 runs, which is reflected in the statistics in Table 4. The mean wave period is predicted less accurately, however, showing an overestimation approaching the partial blocking point. Examination of the frequency spectra reveals that this is due to an exaggerated frequency-downshift of spectral components in SWAN due to the blocking of higher-frequency components (not shown).

For the flume case of Lai et al. (1989), the predictor  $c_{\sigma}/\sigma$  (panel (h)) has positive values where the current gradient is negative (panel (f)), leading to enhanced dissipation, and negative values where the current gradient is positive. As a result, the strong overestimation of significant wave height over the negative current gradient with the default model

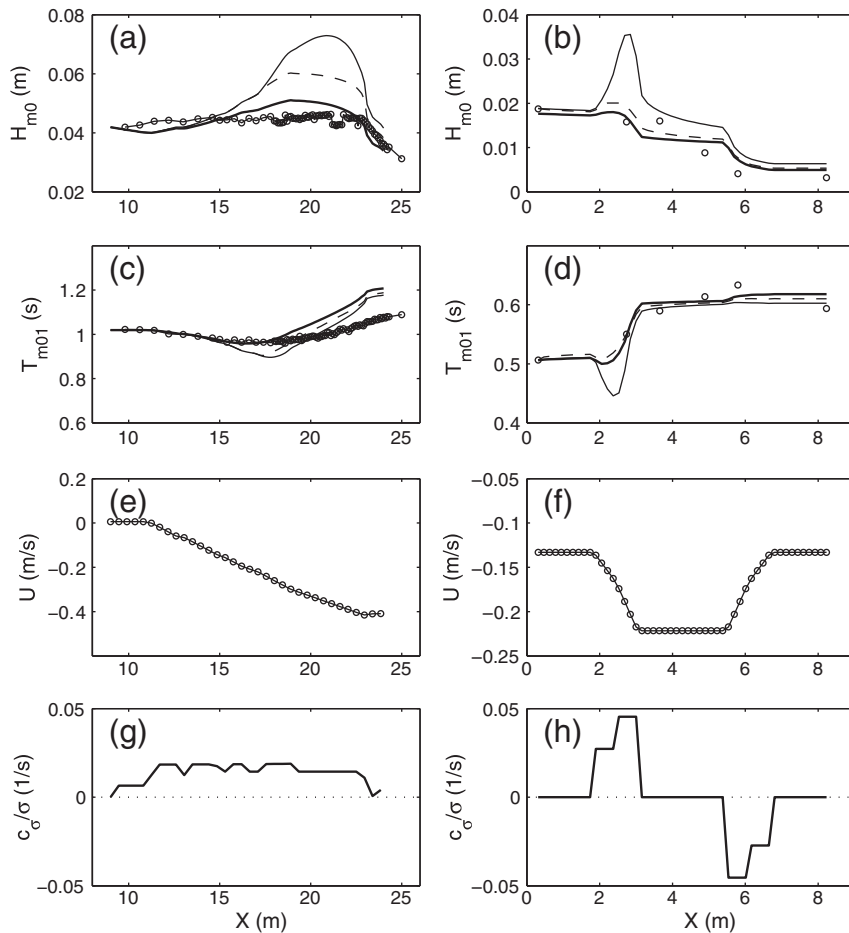


**Fig. 4.** Calibration results of (21) for case I100suast002 of the flume experiment of Suastika (2004) (left, including perforated bottom dissipation) and Lai et al. (1989) (right). Comparison between Van der Westhuysen (2007) (thin solid) whitcapping only, and with RH96 (dashed) and proposed model with  $C_{ds}''=0.65$  (thick solid). Bottom panels show the normalized rate of change in the wave steepness  $c_{\sigma}/\sigma$ .

is corrected using Eq. (21) (panel (b)). In addition, the enhanced dissipation also leads to an improved agreement between the modeled and observed mean period (panel (d)). Both these improvements are similar to those found with the RH96 expression, as can also be seen in the statistics in Table 4. Fig. 5 presents the corresponding frequency spectra for this case at a number of observation stations. Location  $X = 2.74$  m is situated in the strong negative current gradient discussed above, where the default model strongly overestimates the variance density. This overestimation is skewed towards higher frequencies, resulting in the observed underestimation of the mean period. Both the RH96 expression and the proposed formulation Eq. (21) correct this overestimation of the variance. These two model variants generally reproduce the observed spectra well, although some remaining overestimation is found towards the end of the flume.

#### 4. Validation

In this section, the performance of the calibrated expression (21) is evaluated on the basis of the validation data set, and compared with the performance of the RH96 expression. The model performance is first assessed for idealized fetch-limited wave growth without current. This is done in order to verify the desired characteristic that the expression for enhanced current-induced dissipation should not affect model results in the absence of ambient current. Subsequently, the proposed expression is validated for the complex field situation of the Amelander Zeegat.

#### 4.1. Idealized fetch-limited wave growth

Fig. 6 presents simulation results for deep water fetch-limited wave growth, for a wind speed of  $U_{10} = 20$  m/s. The results of three model variants are shown, namely (i) the default model featuring the whitecapping expression of Van der Westhuysen (2007), (ii) the default model with the addition of the enhanced dissipation (21), and (iii) the default model with the addition of the enhanced dissipation proposed by RH96. First, as expected, Fig. 6 shows that the default model produces a satisfactory growth curve through the observations of Kahma and Calkoen (1992). Second, on this scale, the results of the model variant including Eq. (21) cannot be distinguished from those of the default model. This verifies the desired characteristic that the expression for enhanced current-induced dissipation should not affect wave growth results in the absence of ambient current, as is also apparent from inspection of Eq. (21).

By contrast, Fig. 6 shows that the application of the RH96 expression to the default model yields a strong underestimation wave growth for younger wind sea, up to a fetch of about  $X^* = 1 \times 10^6$ . This result is analogous to that presented by Ris (1997), who used Komen et al. (1984) whitecapping as basis. Ris (1997) showed that this spurious model performance is due to excessive dissipation of steep young waves by the RH96 expression. The length scales over which this underestimation of wave growth occurs are relevant for the Wadden Sea situation, in particular for local wind sea growth in the Wadden Sea interior, as will be shown below.

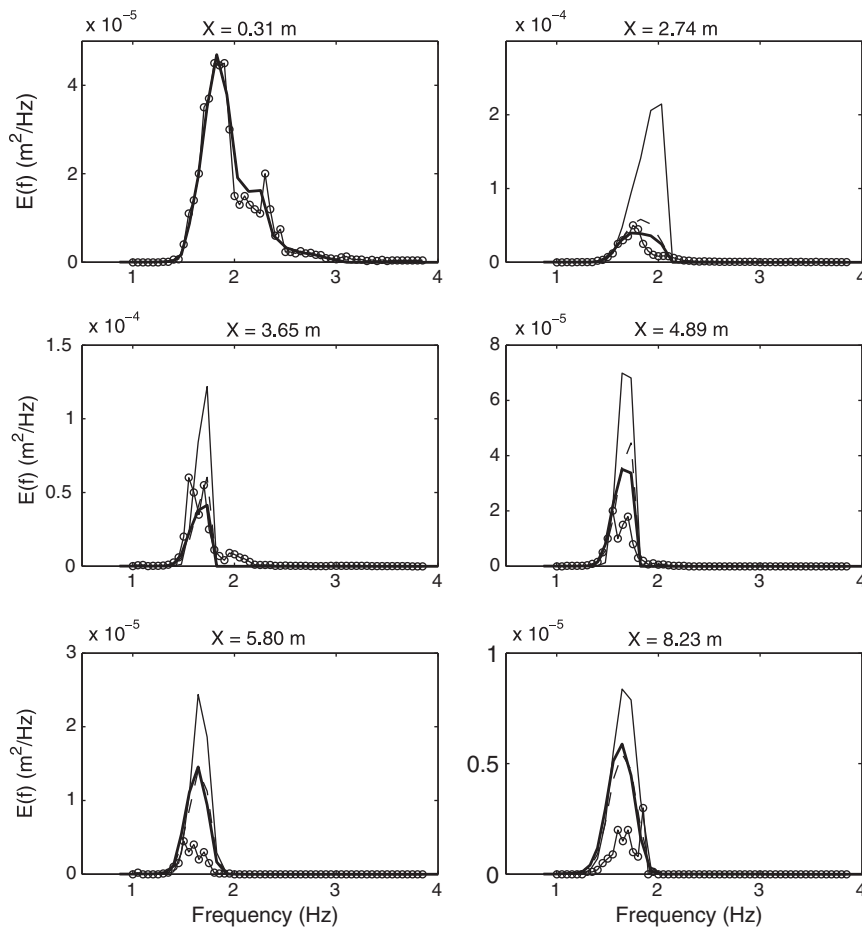
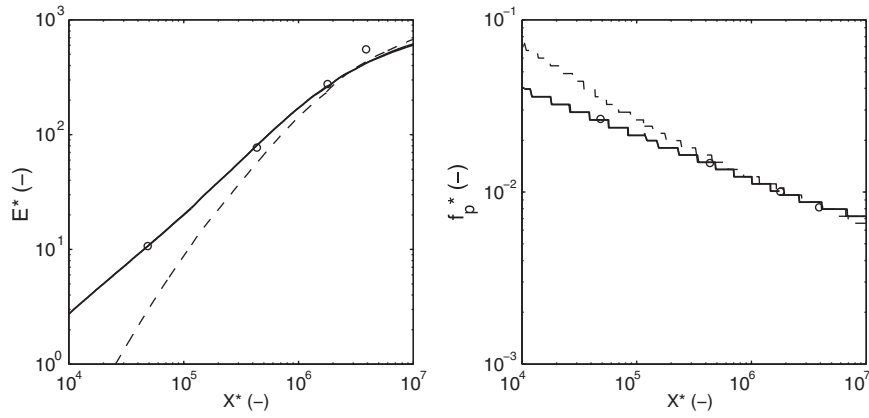


Fig. 5. Frequency spectra results for the partial blocking case of Lai et al. (1989) at six locations along the flume. Comparison between Van der Westhuysen (2007) (thin solid) whitecapping only, and with RH96 (dashed) and proposed model with  $C_{ds}^* = 0.65$  (thick solid). Observed variance densities indicated by line with circles. Note the variation in vertical scale at the various locations.



**Fig. 6.** Fetch-limited wave growth curves for the Van der Westhuysen (2007) whitecapping (thin solid), and with additional enhanced whitecapping according to RH96 (dashed) and proposed expression (thick solid). Note that the latter is indistinguishable from the original Van der Westhuysen (2007) result at this scale. Observations of Kahma and Calkoen (1992) indicated by circles, with  $X^* = gX/u_c^2$ ,  $E^* = g^2E/u_c^4$  and  $f_p^* = u_c f_p/g$ .

4.2. Amelander Zeegat validation subset

The model performance is subsequently considered for the validation subset featuring NW and W storms recorded in the Amelander Zeegat inlet in 2007. The conditions in these cases are equally distributed between opposing and following current in the inlet, with a number of opposing current cases exceeding 1 m/s. Scaled with the wave group velocity, maximum opposing relative current speeds of around  $U/c_{g,peak} = 0.4$  are found, thus corresponding to partially blocking conditions.

Fig. 7 compares model results in the tidal channel (buoys AZB32/42/52) with observations in terms of scatter plots of  $H_{m0}$ ,  $T_{m-1,0}$  and the non-dimensional ratio  $H_{m0}/d$ . These parameters have been computed for the frequency range 0.03–0.5 Hz. The left-hand column presents the results of the default model, featuring the whitecapping expression of Van der Westhuysen (2007). Although the general agreement between the model results and the observations is good, the wave heights in the tidal channel are overestimated by an average of 9%. For conditions with negative current gradients, this is related to insufficient dissipation of waves steepening in the current, as illustrated by the flume

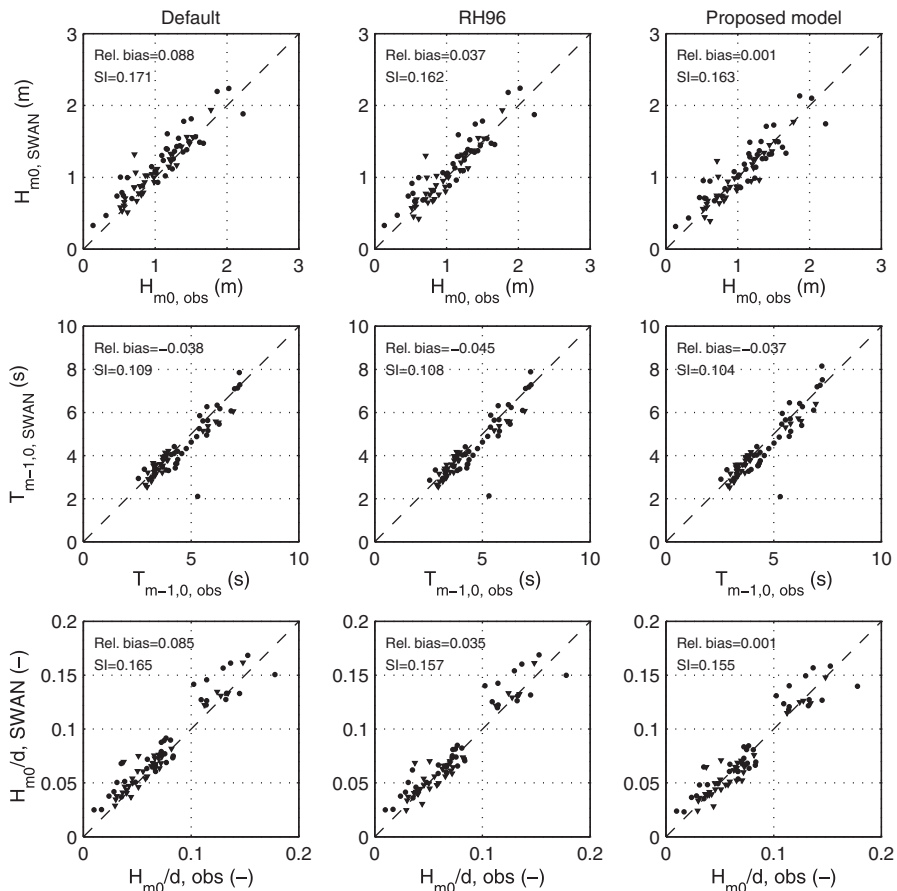


**Fig. 7.** Scatter plot results for the Amelander Zeegat validation cases. Comparison between Van der Westhuysen (2007) whitecapping only (left column), and with RH96 (center) and proposed model with  $C_{d_s} = 0.65$  (right). Shown are results of Jan/Mar 2007 (inverted triangles) and Nov 2007 (circles) for the buoys AZB32/42/52 in the tidal channel.

cases above. The results for the mean period show good agreement with the observations. The results of the  $H_{m0}/d$  ratio in the tidal channel, in relatively deep water ( $H_{m0}/d < 0.2$ ), reflect those of the significant wave height  $H_{m0}$  with an overestimation of 9%. The center column of Fig. 7 presents the simulation results of the default model including the additional expression of RH96. With this additional term, the overestimation of the significant wave height and the  $H_{m0}/d$  ratio at the channel buoys is reduced to 4%, with only a slight deterioration of the mean period results.

The right-hand column of Fig. 7 presents the corresponding results for the default model in combination with the enhanced dissipation (21), using the calibrated value  $C_{ds}^* = 0.65$ . For the channel buoys AZB32/42/52, the 9% overestimation in  $H_{m0}$  and the  $H_{m0}/d$  ratio found with the default model is now corrected. The improvement is the most pronounced for the cases of the November 2007 storm, for which a number of data points were overestimated using the default model. For the Jan/Mar 2007 storms, similar, although less pronounced, improvement in predicted significant wave heights is seen. The good agreement between modeled and observed mean period found with the default model is retained.

Fig. 8 presents the corresponding results for all buoys in the Amelander Zeegat study domain, with the channel buoys discussed above indicated by filled symbols. Considering this total data set, the relatively small negative bias in significant wave height of 3% is increased to a negative bias of 9% with the inclusion of the RH96 term and 8% with expression (21). As above, the mean period results show only minor sensitivity to the additional dissipation terms. The most significant difference between the three model versions is seen in the results of the  $H_{m0}/d$  ratio at the buoys in the shallow interior (AZB41/51/61/62). At these buoys, the model version including the RH96 term show

a strong underestimation of this parameter (bottom center panel). At these buoys, steep, young wind sea is excessively dissipated by the RH96 term, as was found in the fetch-limited growth curve results in Fig. 6 above. As a result, the overall statistics of this model variant are poorer than those of the default model. By contrast, application of Eq. (21) does not lead to the strong deterioration in  $H_{m0}/d$  results for younger wind sea over the tidal flats found with the RH96 expression. This is due to the fact that the enhanced dissipation term Eq. (21) isolates the steepening due to the current gradient. Nonetheless, with the inclusion of Eq. (21) the overall error statistics of both  $H_{m0}$  and  $H_{m0}/d$  show a greater negative bias than those of the default model. This occurs because some negative current gradients are present over the tidal flats, which enhances the dissipation of the young wind sea there (see Fig. 11 below). In recent studies by Zijlema et al. (2012) and Van der Westhuysen et al. (in review) the negative model bias over the inner tidal flats have been addressed by a revision to the proportionality coefficient of the Hasselmann et al. (1973) bottom friction term in (5) from the default  $C_{f, JON} = 0.067 \text{ m}^2/\text{s}^3$  to  $C_{f, JON} = 0.038 \text{ m}^2/\text{s}^3$ .

Fig. 9 shows examples of the frequency spectra at the wave buoys AZB32 and AZB42 in the main tidal channel and AZB41 on the tidal flats, away from the tidal current, produced by the three model variants under ebb conditions (opposing current). At AZB32 and AZB42, the default model overestimates the wind sea portion of the spectrum in the negative current gradient caused by the ebb flow in the inlet. This occurs despite the fact that the mean direction and directional spread are adequately reproduced. Application of the RH96 enhanced dissipation expression yields some improvement, but still overestimates the observed variance. By contrast, at the buoy AZB41, located on the tidal flats, the RH96 model significantly underestimates the growth of the young wind sea, as was seen in the scatter plots above. The model run

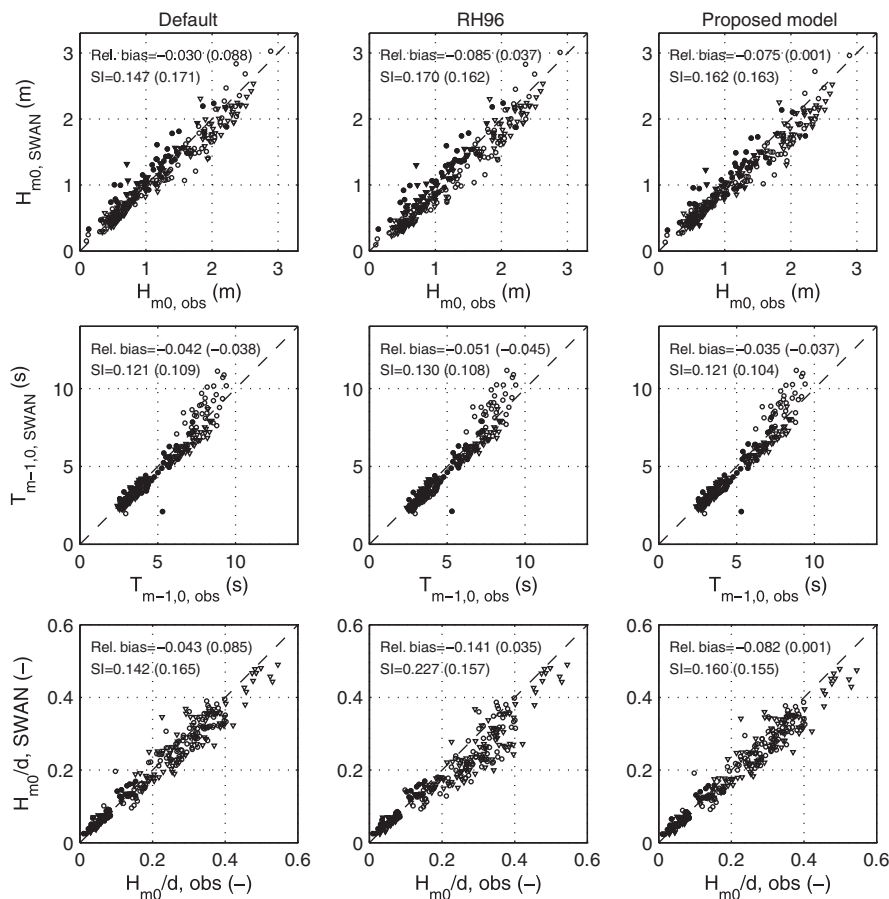
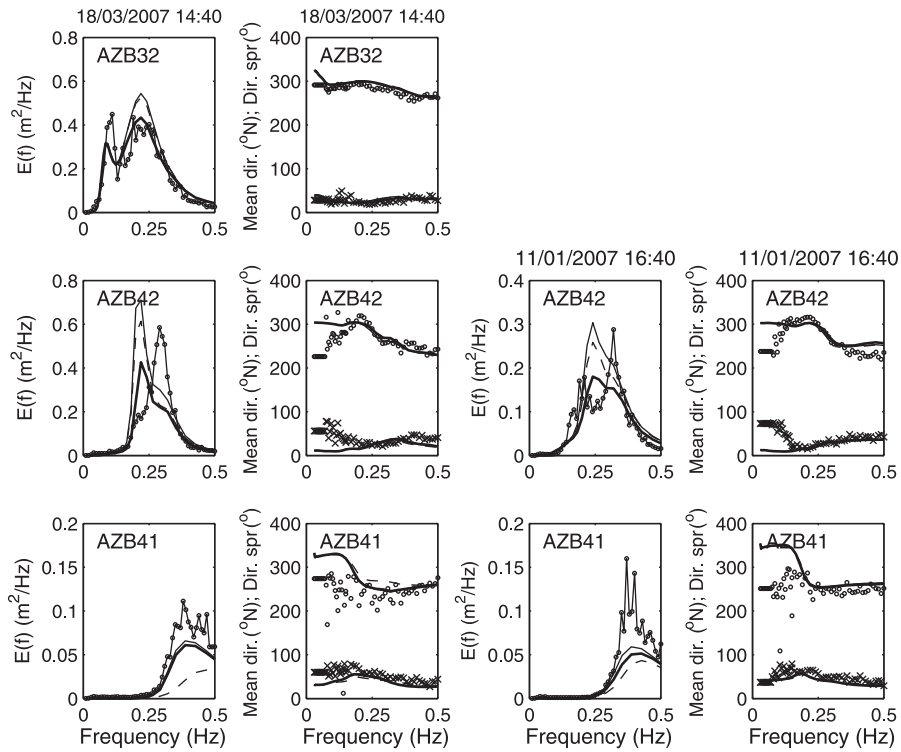


Fig. 8. As in Fig. 7, but now for all buoys, with error statistics given outside of the parentheses. Buoys AZB32/42/52 in the tidal channel have filled symbols, and their statistics are repeated inside the parentheses.



**Fig. 9.** Frequency spectra results, including mean direction and directional spread, for two Amelander Zeegat stationary cases during ebb (refer Table 3). Results shown for the default (thin solid), RH96 (dashed) and proposed (thick solid) models. Observed variance densities indicated by line with circles, mean direction by circles and directional spread by crosses. Note that results for AZB32 on 11/01/2007 at 16:40 have been omitted due to unavailability of observations.

featuring the enhanced whitcapping expression of Eq. (21) yields a better prediction at AZB32 and AZB42 than either the default or the RH96 variants, although the erroneous frequency downshift in the

model at AZB42 is still not corrected. Furthermore, unlike with the RH96 expression, the results at the shallow water buoy AZB41 are mostly unaffected, as desired.

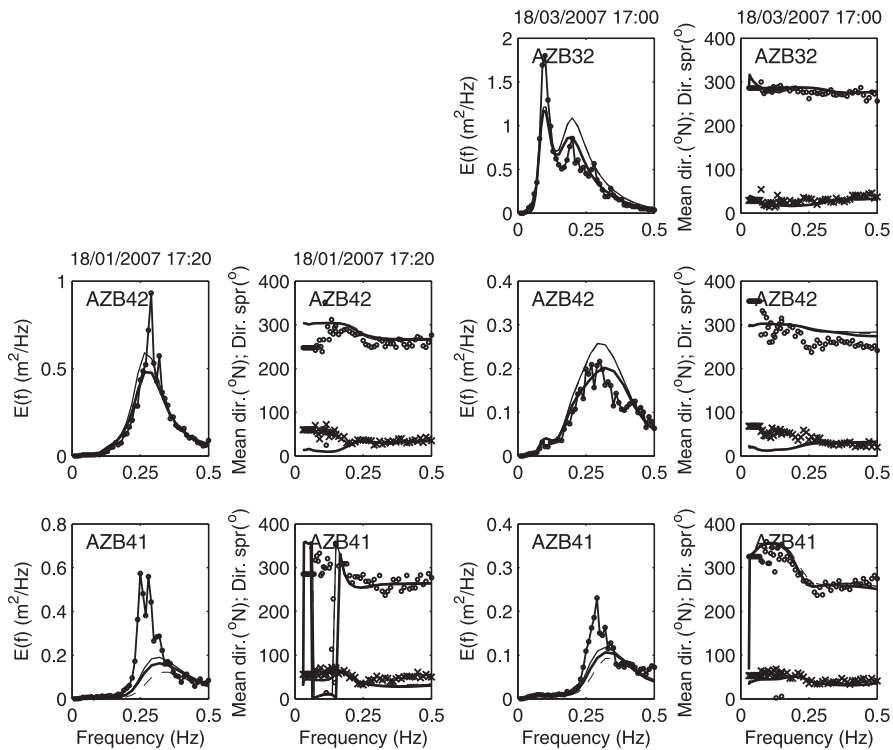


**Fig. 10.** Frequency spectra results, including mean direction and directional spread, for two Amelander Zeegat stationary cases during flood (refer Table 3). Results shown for the default (thin solid), RH96 (dashed) and proposed (thick solid) models. Observations indicated by line with circles, mean direction by circles and directional spread by crosses. Note that results for AZB32 on 18/01/2007 at 17:20 have been omitted due to unavailability of observations.

Fig. 10 shows examples of frequency spectra at AZB32, AZB42 and AZB41 under flood conditions (following current) in the inlet. For these cases, the default model reproduces the observed spectra, including their mean direction and directional spread, generally well. Where waves are elongated under the influence of an accelerating following current (positive current gradient), the formulation Eq. (21) will not have any effect. Indeed, for case f102am7z006 (18/01/2007 17:20) at buoy AZB42, the model results have only a small sensitivity to the application of either the RH96 or the proposed dissipation expressions, as desired. However, for case f102am07z011 (18/03/2007 17:00), waves at AZB32 and AZB42 experience negative current gradients due to decelerating following current, and are dissipated as a result, improving agreement with the observations. However, as seen above, the RH96 expression yields strong underestimations at the buoy AZB41 on the tidal flats. Here the model variant featuring the enhanced dissipation Eq. (21) only has a limited impact on the results at these locations.

Fig. 11 shows the spatial distribution of the effect of the proposed model on the integral parameters  $H_{m0}$  and mean period  $T_{m-1,0}$  for the presented ebb and flood cases. The top left-hand panel of Fig. 11 shows that in the ebb case f102am07z009 (18/03/2007 14:40), the wave heights in the tidal channel diminish by up to 30% due to the enhanced dissipation of Eq. (21) under a large region of negative current gradients in the opposing channel currents. By comparison, the mean period  $T_{m-1,0}$  experiences relatively little change due to the application of Eq. (21) (bottom left-hand panel). It is interesting to observe that in some parts of the tidal inlet the mean period increases due to the enhanced dissipation, for example at AZB32. Inspection of the frequency spectra reveals this to be due to the reduction of the wind sea peak while the lower-frequency peak from the North Sea wave system remains intact (not shown).

The right-hand panels of Fig. 11 show the spatial distribution of the impact of the proposed model Eq. (21) on  $H_{m0}$  and mean period  $T_{m-1,0}$  results for the flood case f102am07z006 (18/01/2007 17:20). The impact on the significant wave height is generally smaller than for the presented ebb case. This is particularly so in the main tidal

channel at the buoys AZB32/42. However, as seen in the frequency spectra results above, the impact of the enhanced dissipation is not negligible everywhere. Inspection of the spatial current pattern (not shown) reveals decelerating following current in this region, but its occurrence is more limited than in the typical ebb case. Hence, some degree of enhanced dissipation is to be expected according to Eq. (21). The bottom right-hand panel of Fig. 11 shows the proposed model to have only a marginal impact on the mean period  $T_{m-1,0}$  results for this flood case.

## 5. Conclusions

The present study aimed to correct the overestimation of wave heights on partially blocking, negative current gradients in SWAN, as found in the tidal channels of the Wadden Sea. This model inaccuracy was addressed by means of the development of a formulation for the enhanced breaking dissipation of waves that is related to the degree of their current-induced steepening. This formulation was calibrated and validated for a range of laboratory and field situations. It should be noted that the expression proposed here is not suited to fully blocking conditions, where nonlinear effects should be taken into account. The following conclusions can be drawn from the results of this study:

1. Using a diverse set of laboratory and field cases, this study shows that when using conventional whitecapping expressions in SWAN, which are calibrated for wind wave growth, significant wave heights are overestimated in the presence of negative current gradients. This confirms earlier results of Ris and Holthuijsen (1996).
2. The results of this study confirm that the addition of enhanced whitecapping dissipation according to Ris and Holthuijsen (1996) improves results for laboratory cases. However, as shown by Ris (1997), this expression leads to underestimation of young wind sea due to their inherent high steepness. This results in significant

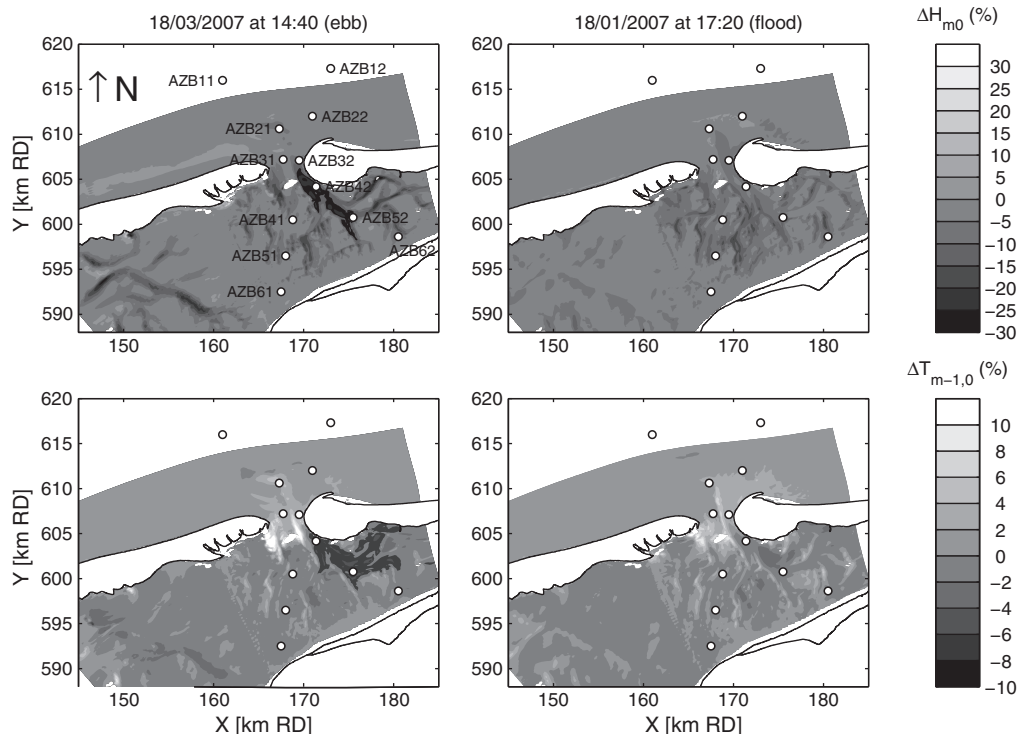


Fig. 11. Impact of proposed model (21) on spatial fields of wave parameters. Left-hand panels: Amelande Zeegat case f102am07z009 (ebb). Right-hand panels: Amelande Zeegat case f102am07z006 (flood).

underestimation of locally-generated wind sea over the tidal flats in the Wadden Sea interior.

3. A new formulation for the enhanced dissipation of waves on negative current gradients is proposed, which is based on the saturation-based formulation of Van der Westhuysen et al. (2007), and scaled with the degree of current-induced steepening of the wave field. The latter is related to the current-induced Doppler shifting per spectral component. This expression contains one additional unknown parameter, which was calibrated to a value of  $C_{ds}^* = 0.65$  using laboratory observations.
4. Validation of the proposed enhanced dissipation term for a data set of Amelande Zeegat field cases shows that the overestimation of significant wave heights at the channel buoys under negative current gradients is corrected. The satisfactory prediction of the mean period  $T_{m-1,0}$  is retained. Importantly, the results for the locally-generated wind sea on the tidal flats are not as strongly affected as with the expression of Ris and Holthuijsen (1996). However, the addition of the proposed dissipation term does increase the negative bias in wave height over the inner tidal flats region found with the default model. Recent studies by Zijlema et al. (2012) and Van der Westhuysen et al. (in review) have indicated that the negative model bias over this region can be corrected by a revision of the appropriate level of bottom friction dissipation.
5. Due to the complex tidal channel system and resulting current patterns in the Wadden Sea, regions of negative current gradients (in the inlet and over the flats) are also found for flood conditions (e.g. decelerating flood currents). Over these areas, the proposed expression for enhanced breaking dissipation results in increased dissipation.

## Acknowledgments

The presented work is part of the SBW (Strength and Loads on Water Defenses) project commissioned by Rijkswaterstaat Centre for Water Management in the Netherlands. The Delft University of Technology is acknowledged for their kind permission to use the data set of Suastika (2004). The author would like to thank Ap van Dongeren and Jacco Groeneweg for their useful comments, and Jurjen Battjes for his conceptual input, including Appendix A, which has resulted in a substantial improvement of an earlier draft of the manuscript.

## Appendix A

In this appendix, by Battjes (2011), the contributions to  $c_{\sigma}$  and the conditions determining its sign, i.e. the right-hand side of Eq. (3) in the main text, are examined.

For stationary conditions, as assumed in the present applications, the first term in the brackets in the right-hand side is zero. The remaining two terms represent the effects of changes in depth following the current, and of varying relative current strength, respectively. Defining  $U_n$  as the velocity component normal to the depth contours, positive in the direction of increasing depth, and  $U_s$  as the current velocity component in the direction of the wave propagation, and omitting the nonstationary term, Eq. (3) can be written as

$$c_{\sigma} = \frac{\sigma k}{\sinh 2kd} U_n |\nabla d| - c_g k \frac{\partial U_s}{\partial s}, \quad (\text{A.1})$$

where  $\partial \sigma / \partial d = \sigma k / \sinh 2kd$ . The balance between these two terms varies with the local conditions, but it can be argued that in general the first term will be far smaller than the second. The model is intended for waves on currents, specifically in the channels. There, the velocity  $U$  is more or less aligned with the depth contours, in which case  $U_n$  is near zero. Moreover, for waves on relatively deep water, as may occur in the major channels, depth variations do not

directly influence the wave propagation. Therefore, with increasing depth, the first term vanishes in proportion to  $1/\sinh 2kd$ .

With respect to the last term on the RHS of (A.1), it is noted that current velocity variations can occur as a result of depth variations, proportional to  $U|\nabla d|$ , but additionally due to lateral divergence or convergence, and as a result of storage (in nonstationary situations). Lastly, the component of velocity in the wave propagation direction can vary as a result of changes in angle between current and waves, even for constant current strength.

For the preceding reasons, the term representing the effects of the depth gradient is believed to be the smallest in most circumstances. Neglecting it, Eq. (A.1) reduces to

$$c_{\sigma} \cong -c_g k \frac{\partial U_s}{\partial s}. \quad (\text{A.2})$$

The sign of this expression, and therefore the associated occurrence of enhanced dissipation in the model, does not depend on that of  $U_s$  (following or opposing current) but on its gradient in the wave propagation direction,  $\partial U_s / \partial s$ . Negative values of  $\partial U_s / \partial s$  (implying enhanced dissipation in the model) occur on an opposing current where this increases in strength in the propagation direction, but also on a following current where this is decreasing in strength in the propagation direction.

Physically, the enhanced dissipation according to the proposed model occurs where the waves are shortening as they propagate ( $d\sigma/dt > 0$ ), in other words, in a region where they are decelerating. It is clear that this not only occurs where the waves run on a counter current of increasing strength, but also on a following current of decreasing strength.

The direct contribution by the depth gradient has been neglected to arrive at Eq. (27). Taking that contribution into account will modify the results to some extent. Depending on the local conditions, it can strengthen the effect of the downwave variations in the downwave current velocity, or it can oppose that effect.

## References

- Alves, J.H.G.M., Banner, M.L., 2003. Performance of a saturation-based dissipation-rate source term in modelling the fetch-limited evolution of wind waves. *Journal of Physical Oceanography* 33, 1274–1298.
- Ardhuin, F., Rogers, W.E., Babanin, A.V., Filipot, J.-F., Magne, R., Roland, A., van der Westhuysen, A.J., Queffelec, P., Lefevre, J.-M., Aouf, L., Collard, F., 2010. Semi-empirical dissipation source functions for ocean waves: Part I, definitions, calibration and validations. *Journal of Physical Oceanography* 40 (9), 1917–1941. <http://dx.doi.org/10.1175/2010JPO4324.1>.
- Babanin, A.V., Tsagareli, K.N., Young, I.R., Walker, D.J., 2010. Numerical investigation of spectral evolution of wind waves. Part II: dissipation term and evolution tests. *Journal of Physical Oceanography* 40, 667–683. <http://dx.doi.org/10.1175/2009JPO4370.1>.
- Babanin, A.V., Hwung, H.-H., Shugan, I., Roland, A., van der Westhuysen, A., Chawla, A., Gautier, C., 2011. Nonlinear Waves on Collinear Currents with Horizontal Velocity Gradient. Proc. 12th Int. Workshop on Wave Hindcasting and Forecasting. <http://www.waveworkshop.org/12thWaves/index.htm>.
- Battjes, J.A., 2011. Personal communication, July 2011.
- Battjes, J.A., Janssen, J.P.F.M., 1978. Energy Loss and Set-up Due to Breaking of Random Waves. Proc. 16th Int. Conf. Coastal Eng., ASCE, pp. 569–588.
- Booij, N., Ris, R.C., Holthuijsen, L.H., 1999. A third generation wave model for coastal regions, Part I, Model description and validation. *Journal of Geophysical Research* 104 (C4), 7649–7666.
- Chawla, A., Kirby, J.T., 1998. Experimental Study of Wave Breaking and Blocking on Opposing Currents. Proc. 26th Int. Conf. Coastal Eng., ASCE, pp. 759–772.
- Chawla, A., Kirby, J.T., 2002. Monochromatic and random wave breaking at blocking points. *Journal of Geophysical Research* 107 (C7). <http://dx.doi.org/10.1029/2001JC001042>.
- Eldeberky, Y., 1996. Nonlinear transformations of wave spectra in the nearshore zone. Ph.D Thesis, Fac. of Civil Engineering, Delft University of Technology, 203 pp.
- Groeneweg, J., van der Westhuysen, A.J., van Vledder, G.P., Jacobse, S., Lanser, J., van Dongeren, A.R., 2008. Wave Modelling in a Tidal Inlet: Performance of SWAN in the Wadden Sea. Proc. 31th Int. Conf. Coastal Eng., ASCE, pp. 411–423.
- Hasselmann, K., Barnett, T.P., Bouws, E., Carlson, H., Cartwright, D.E., Enke, K., Ewing, J.A., Gienapp, H., Hasselmann, D.E., Kruseman, P., Meerburg, A., Müller, O., Olbers, D.J., Richter, K., Sell, W., Walden, H., 1973. Measurement of windwave growth and swell decay during the Joint North Sea Wave Project (JONSWAP). *Deutsche Hydrographische Zeitschrift* 8 (12) (Suppl., A 95 pp.).

- Hasselmann, S., Hasselmann, K., Allender, J.A., Barnett, T.P., 1985. Computations and parameterizations of the nonlinear energy transfer in a gravity-wave spectrum. Part 2: parameterization of the nonlinear transfer for application in wave models. *Journal of Physical Oceanography* 15, 1378–1391.
- Haus, B.K., 2007. Surface current effects on the fetch-limited growth of wave energy. *Journal of Geophysical Research* 112, C03003. <http://dx.doi.org/10.1029/2006JC003924>.
- Holthuijsen, L.H., Tolman, H.L., 1991. Effects of the Gulf Stream on ocean waves. *Journal of Geophysical Research* 96, 12755–12771.
- Holthuijsen, L.H., Herman, A., Booij, N., 2003. Phase-decoupled refraction–diffraction for spectral wave models. *Coastal Engineering* 49, 291–305.
- Jonsson, I.G., 1990. Wave-current interaction. In: LeMéhauté, B., Hanes, D. (Eds.), *The Sea: Ocean Engineering Science*, vol. 9B. John Wiley, Hoboken, NJ, pp. 65–120.
- Kahma, K.K., Calkoen, C.J., 1992. Reconciling discrepancies in the observed growth of wind-generated waves. *Journal of Physical Oceanography* 22, 1389–1405.
- Kirby, J.T., Dalrymple, R.A., 1986. An approximate model for nonlinear dispersion in monochromatic wave propagation models. *Coastal Engineering* 9, 545–561.
- Komen, G.J., Hasselmann, S., Hasselmann, K., 1984. On the existence of a fully developed wind-sea spectrum. *Journal of Physical Oceanography* 14, 1271–1285.
- Lai, R.J., Long, S.R., Huang, N.E., 1989. Laboratory studies of wave-current interaction: kinematics of the strong interaction. *Journal of Geophysical Research* 94, 16,201–16,214.
- Mei, C.C., 1983. *The applied dynamics of ocean surface waves*. Wiley, New York, 740 pp.
- Phillips, O.M., 1985. Spectral and statistical properties of the equilibrium range in wind-generated gravity waves. *Journal of Fluid Mechanics* 156, 505–531.
- Ris, R.C., 1997. Spectral modelling of wind waves in coastal waters, Ph.D Thesis, Fac. of Civil Eng., Delft Univ. of Tech., 160 pp.
- Ris, R.C., Holthuijsen, L.H., 1996. Spectral Modelling of Current Wave-blocking. Proc. 25th Int. Conf. on Coastal Eng., ASCE, pp. 1247–1254.
- Suastika, I. K., 2004. Wave blocking, Ph.D Thesis, Fac. of Civil Eng., Delft Univ. of Tech., 157 pp.
- Suastika, I.K., de Jong, M.P.C., Battjes, J.A., 2000. Experimental Study of Wave Blocking. Proc. 27th Int. Conf. on Coastal Eng., ASCE, pp. 227–240.
- Thornton, E.B., Guza, R.T., 1983. Transformation of wave height distribution. *Journal of Geophysical Research* 88, 5925–5938.
- Van der Westhuysen, A. J., 2007. Advances in the spectral modelling of wind waves in the nearshore, Ph.D Thesis, Fac. of Civil Eng., Delft Univ. of Tech., 207 pp.
- Van der Westhuysen, A.J., 2009. Modelling of Depth-Induced Wave Breaking Over Sloping and Horizontal Beds. Proc. 11th Int. Workshop on Wave Hindcasting and Forecasting. <http://www.waveworkshop.org/11thWaves/Papers>.
- Van der Westhuysen, A.J., 2010. Modelling of depth-induced wave breaking under finite-depth wave growth conditions. *Journal of Geophysical Research* 115, C01008. <http://dx.doi.org/10.1029/2009JC005433>.
- Van der Westhuysen, A.J., Zijlema, M., Battjes, J.A., 2007. Nonlinear saturation-based whitecapping dissipation in SWAN for deep and shallow water. *Coastal Engineering* 54, 151–170.
- Van der Westhuysen, A. J., A. R. van Dongeren, J. Groeneweg, G. Ph. van Vledder, H. Peters, C. Gautier and J. C. C. van Nieuwkoop, in review. Improvements in spectral wave modeling in tidal inlet seas. *Journal of Geophysical Research*.
- Van Vledder, G.P., Groeneweg, J., van der Westhuysen, A.J., 2008. Numerical and Physical Aspects of Wave Modelling in a Tidal Inlet. Proc. 31th Int. Conf. Coastal Eng., ASCE, pp. 424–436.
- Whitham, G.B., 1974. *Linear and nonlinear waves*. John Wiley and Sons, New York, 636 pp.
- Yan, L., 1987. An Improved Wind Input Source Term for Third Generation Ocean Wave Modelling. Technical Report No. 87–8. Royal Dutch Meteor. Inst. (KNMI).
- Zijderveld, A., Peters, H., 2008. Measurement Programme Dutch Wadden Sea. Proc. 31th Int. Conf. Coastal Eng., ASCE, pp. 404–410.
- Zijlema, M., G. Ph. van Vledder and L.H. Holthuijsen, 2012. Bottom friction and wind drag for wave models. *Coastal Engineering* 65, 19–26.
- Zijlema, M., van der Westhuysen, A.J., 2005. On convergence behaviour and numerical accuracy in stationary SWAN simulations of nearshore wind wave spectra. *Coastal Engineering* 52, 237–256.